npj | climate and atmospheric science **Article**

Published in partnership with CECCR at King Abdulaziz University

https://doi.org/10.1038/s41612-025-01133-6

Enhanced oxidation capacity driven by pollution-induced chlorine chemistry in the coastal atmosphere

Gaojie Chen[1,2,3], **Ziying Chen**[1,2,3], **Yanru Zhang**[4], **Xiaolong Fan**[1,2], **Lingling Xu**[1,2] ✉, **Ziyi Lin**[1,2,3], **Xiaoting Ji**[1,2,3] & **Jinsheng Chen**[1,2] ✉

Reactive chlorine chemistry strongly influences the regulation of atmospheric oxidation capacity, thereby exerting profound impacts on the formation of secondary pollutants and air quality. However, current understanding of distributions and formation mechanisms of reactive chlorine species under the influence of air masses induced by pollution remains limited. In this study, we observed a significant increase in the concentrations of $ClNO_2$, Cl_2, and HOCl driven by pollution under the influence of continental air masses. By integrating field observations with model simulations, we revealed that unknown sources of these chlorine species are associated with nitrate photolysis and aerosol iron-mediated photochemical processes. The elevated levels of chlorine species promoted the increase in RO*x* radical concentrations, considerably intensifying the chemical formation of O_3 and PAN and changing their sensitivity. These findings highlight the importance of anthropogenic pollutants in driving chlorine chemistry and provide scientific insights into its significance in regulating photochemical pollution.

Chlorine radicals (Cl·) are an important atmospheric oxidant, affecting atmospheric chemical components and deteriorating air quality[1–4]. In the polluted troposphere, Cl· can react with volatile organic compounds (VOCs), resulting in the formation of primary RO*x* radicals (including OH·, HO_2·, and RO_2·) and O_3, thereby enhancing atmospheric oxidation capacity[5–7].

Nitryl chloride ($ClNO_2$) and molecular chlorine (Cl_2) are the major Cl· precursors in the troposphere and have been investigated on a global scale[5,8–19]. $ClNO_2$ is generally generated through the heterogeneous uptake of dinitrogen pentoxide (N_2O_5) on the chloride-containing aerosols[8], with its highest levels occurring after sunset and photolyzing rapidly after sunrise[7,20]. However, high daytime concentrations of $ClNO_2$ have also been observed in previous research, mainly due to transport from upper atmosphere or reduced photolysis rates[6,17,21]. Cl_2 can be produced from both primary and secondary sources[12,18,22], with peak concentrations occurring either during the daytime or nighttime[5,23,24]. During the daytime, photochemical processes within aerosol particles, such as those associated with O_3[25–27], OH·[28], Fe(III)[29], nitrates[18], titanium dioxide (TiO_2)[30], $ClNO_2$[31,32], hypochlorous acid (HOCl)[33], and chlorine nitrates ($ClONO_2$)[34] on chloride-containing aerosols, are considered as important sources of Cl_2. At night, heterogeneous reactions of N_2O_5 also contributed to Cl_2 generation in addition to $ClNO_2$[23,35]. Besides $ClNO_2$ and Cl_2, HOCl is also a daytime source of Cl·[36]. It is generally produced by the reaction of ClO and HO_2·, which did not fully account for the observed HOCl levels in the eastern tropical Atlantic[33]. Recent research suggested that the HOCl levels can be explained by a mix of Saharan dust and sea spray aerosols activated by sunlight[37]. Even nitrate photolysis also contributed to daytime HOCl generation[36].

Currently, numerous observational studies have been conducted on the distribution characteristics and sources of individual chlorine species ($ClNO_2$ or Cl_2)[6,7,18,19,21,23], but the distributions and formation mechanisms of multiple reactive chlorine species (e.g., $ClNO_2$, Cl_2, and HOCl) are not well understood. Previous studies have found that during the COVID-19 lockdown, the reduction in anthropogenic activities led to a sharp decline in NO concentrations, resulting in significant increases in $ClNO_2$ and Cl_2 levels[35]. Another study indicated that the rise in vehicle emissions enhanced nitrogen-related chemical processes associated with NO_2 concentrations after the Spring Festival, further increasing the levels of $ClNO_2$ and Cl_2·[38]. These findings highlight the critical regulatory role of anthropogenic activity-driven chemical processes in the formation and transformation of reactive chlorine species.

Coastal regions influenced by anthropogenic activities and sea-salt aerosols have witnessed emerging insights into the sources of reactive

---

[1]State Key Laboratory of Advanced Environmental Technology, Institute of Urban Environment, Chinese Academy of Sciences, Xiamen, China. [2]Fujian Key Laboratory of Atmospheric Ozone Pollution Prevention, Institute of Urban Environment, Chinese Academy of Sciences, Xiamen, China. [3]University of Chinese Academy of Sciences, Beijing, China. [4]Xiamen Environmental Monitoring Station, Xiamen, China. ✉e-mail: linglingxu@iue.ac.cn; jschen@iue.ac.cn

chlorine species. Our previous autumn observations revealed that nitrate photolysis and aerosol iron photochemical processes serve as major sources of Cl_2 and HOCl at coastal sites[36,39]. Similar with these findings, field measurements coupled with simulations in the coastal atmospheres of Hong Kong further underscore the key contribution of nitrate photolysis to Cl_2 production[18,40], yet the sources of HOCl remain unresolved[40]. Given the complex interplay between marine and continental air masses in coastal environments, systematic investigations under varying air mass conditions are urgently needed to elucidate the formation mechanisms and atmospheric impacts of reactive chlorine species.

In this study, we conducted intensive observations of reactive chlorine species ($ClNO_2$, Cl_2, and HOCl) during summer in a southeastern coastal city. The results indicated that the concentrations of $ClNO_2$, Cl_2, and HOCl were very low under the influence of marine air masses, whereas under the influence of continental air masses, the concentrations of these chlorine species increased sharply, accompanied by secondary pollution. Through the combination of field observations and model simulations, we elucidated the distribution patterns, formation and loss processes, and differential impacts on atmospheric oxidation capacity of $ClNO_2$, Cl_2, and HOCl under the influence of marine and continental air masses. This study not only advances the scientific understanding of the formation mechanisms of multiple reactive chlorine species but also provides important insights for formulating regional photochemical pollution control strategies.

Results and discussion

Significant enhancement of chlorine chemistry

Figure S1 presents the time series of $ClNO_2$, Cl_2, HOCl, and related parameters observed in a coastal city of southeastern China from July 19th to August 9th. Interestingly, the study site was alternately influenced by marine air masses (Type 1) and continental air masses (Type 2) during the observation period from mid-July to early August (Fig. 1a, b). This provided a unique opportunity to investigate the influence of marine and continental air masses on the distributions of reactive chlorine species.

Under the influence of marine air masses, particulate chloride (Cl^-) exhibited a strong correlation with sodium ions (Na^+) (Fig. S2a, r = 0.86) but no significant correlation with potassium ions (K^+) (Fig. S2b, $r = 0.06$). In contrast, during the continental air mass influence period, the correlation between Cl^- and K^+ became statistically significant ($r = 0.49$) (Fig. S2d). This difference confirms that the study site was predominantly influenced by marine and continental air masses during the Type 1 and Type 2 periods, respectively. Notably, the diurnal variation of Cl^- concentrations during the Type 2 period exhibited lower daytime levels (Fig. S3), suggesting the enhanced photochemical loss, which likely promoted the formation of gaseous reactive chlorine species ($ClNO_2$, Cl_2, and HOCl). The average hourly concentrations of $ClNO_2$, Cl_2, and HOCl during the Type 1 period were 0.69, 1.7, and 4.8 ppt, respectively, while during the Type 2 period, they increased markedly to 21.5, 14.3, and

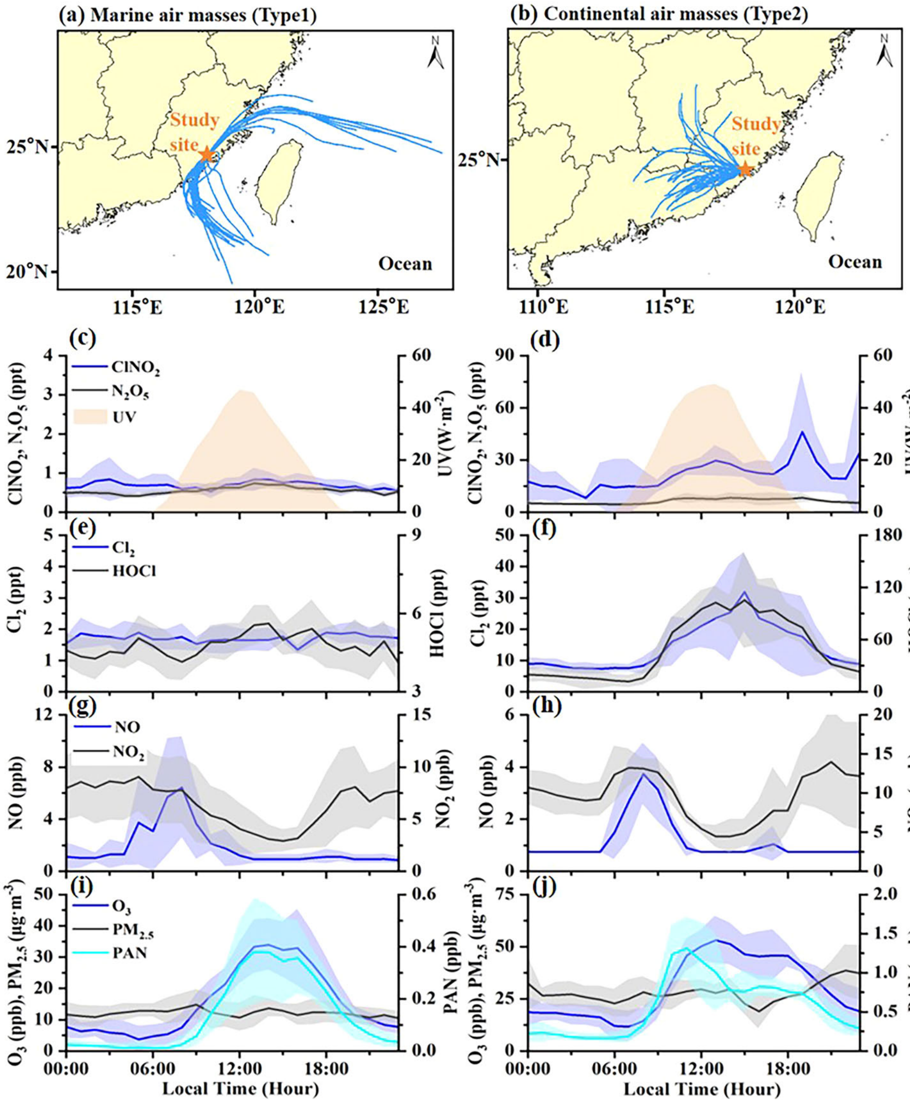

Fig. 1 | Distribution characteristics of reactive chlorine species ($ClNO_2$, Cl_2, and HOCl) and related parameters under the influence of marine and continental air masses, respectively. (**a**, **c**, **e**, **g**, **i**) Period of marine air mass influence (July 19th–26th, 2023); (**b**, **d**, **f**, **h**, **j**) Period of continental air mass influence (August 1st–9th, 2023).

49.9 ppt, respectively (Fig. 1 and Table S1). Concurrently, substantial increases were observed in the concentrations of O_3, PAN, and $PM_{2.5}$, with $PM_{2.5}$ levels rising from a maximum of 20 $\mu g \cdot m^{-3}$ during the Type 1 period to 60 $\mu g \cdot m^{-3}$ during the Type 2 period, reflecting a pronounced deterioration in air quality during the Type 2 period at the study site.

During the Type 1 period, the concentrations of reactive chlorine species were consistently low and exhibited no significant diurnal variations. However, during the Type 2 period, $ClNO_2$ displayed a distinctive diurnal variation pattern characterized by a nighttime peak and sustained elevated levels in the afternoon. We can exclude instrumental artifacts as an explanation for the summer $ClNO_2$ distribution, as evidenced by the characteristic isotopic signature of $ClNO_2$ (Fig. S4). Prior observations reported nighttime peaks and accumulations in $ClNO_2$ concentrations followed by rapid photolysis after sunrise[5,8,13,19]. In this study, the limited nocturnal accumulation of $ClNO_2$ weakened its impact on daytime $ClNO_2$ levels, thereby facilitating the identification of other possible processes related to daytime $ClNO_2$ generation. As indicated by prior studies[41–43], the daytime availability of NO_3 influences $ClNO_2$ concentrations by modulating the formation of N_2O_5 (Fig. S5). Using a box model, we quantitatively assessed the contribution of heterogeneous N_2O_5 uptake to daytime $ClNO_2$ concentrations (Text S1). In our calculations, we adopted an N_2O_5 uptake coefficient ($\gamma(N_2O_5)$) of 0.03 and a $ClNO_2$ production efficiency ($\phi(ClNO_2)$) of 0.6, representing moderate estimates[6,32,44,45]. The simulated daytime $ClNO_2$ levels accounted for only 20% of the observed $ClNO_2$ concentrations (Fig. S6). Even when extreme values of $\gamma(N_2O_5)$ (0.06) and $\phi(ClNO_2)$ (1.0) were applied, the observed daytime $ClNO_2$ peak could not be fully explained by N_2O_5 chemistry alone (Fig. S6), suggesting the existence of unknown daytime $ClNO_2$ formation pathways. Additionally, Cl_2 and HOCl also exhibited daytime peaks. The persistent daytime peaks during the Type 2 period suggest that, despite rapid photolysis, the sources of reactive chlorine species were very strong, continuously replenishing their concentrations. Furthermore, statistical analysis of daytime data (07:00–17:00 Local Time) during the Type 2 period revealed the strong linear correlations among these species: the correlation coefficient (r) between Cl_2 and $ClNO_2$ was 0.75, between HOCl and Cl_2 was 0.66, and between HOCl and $ClNO_2$ was 0.82 (Fig. S7), respectively, implying their common sources.

To investigate the reasons for the elevated concentrations of reactive chlorine species during the Type 2 period, we compared meteorological parameters and related species between the two periods (Table S1). The results showed that photochemical reaction conditions (temperature, UV radiation, and JNO_2 values) and diffusion conditions (wind speed) differed only slightly, suggesting that these meteorological factors were not the primary drivers of the significant differences in the concentrations of reactive chlorine species. However, NO_x levels, aerosol iron (Fe), particle-related components, such as nitrates (NO_3^-) and ammonium (NH_4^+), all exhibited higher concentrations during the Type 2 period. Given the observed daytime concentration peaks of $ClNO_2$, Cl_2, and HOCl, coupled with their short photochemical lifetimes in summer, $ClNO_2$, Cl_2, and HOCl production may be predominantly driven by local photochemical processes. Therefore, the impacts of marine and continental air masses on the concentrations of $ClNO_2$, Cl_2, and HOCl may be indirect, primarily through influencing precursor concentrations rather than directly changing the concentrations of $ClNO_2$, Cl_2, and HOCl. Based on the comprehensive analysis, it is inferred that under the similar conditions of photochemical reaction and atmospheric diffusion, the elevated concentrations of both primary and secondary pollutants during the Type 2 period are likely to facilitate the enhancement of $ClNO_2$, Cl_2, and HOCl production. Pollution-driven chlorine activation was also observed in coastal areas of Hong Kong[18,40]. These results underscore the need for further investigation into the sources and mechanisms driving the formation of daytime reactive chlorine species.

Production and loss processes of reactive chlorine species

Due to the considerable enhancement in the concentrations of reactive chlorine species during the Type 2 period, this study focused on exploring the sources of daytime Cl_2, HOCl, and $ClNO_2$ during this period.

In the box model, Cl_2 concentrations were simulated by incorporating gas-phase reactions (e.g., ClO + ClO and ClO_2 + Cl·) and heterogeneous uptake reactions of $ClNO_2$, HOCl, O_3, and OH· on chloride-containing aerosol surfaces, alongside loss pathways such as Cl_2 photolysis, Cl_2 + OH·, and negligible deposition. Despite including these reactions, the simulated Cl_2 concentrations accounted for only 30% of the observed concentrations (Fig. 2a), implying substantial uncertainties in the uptake coefficients of known pathways or the presence of significant unknown sources. Among the known Cl_2 formation pathways (Fig. 2b), O_3 uptake was the dominant contributor (60.0%), followed by $ClNO_2$ (28.0%) and HOCl (11.0%) uptake, while OH· uptake (<2.0%) and gas-phase reactions played minor roles. Previous studies have demonstrated that incorporating the heterogeneous uptake reaction of O_3 ($\gamma O_3 = 1 \times 10^{-3}$) into the CMAQ model could explain over 80% of Cl_2 formation[46], but the selection of uptake coefficients requires further validation. Given that photolysis is the primary daytime loss pathway for Cl_2 and its photolysis lifetime is short, Cl_2 is generally considered to be in a quasi-steady state, where its production rates approximate its loss rates. By subtracting the total loss rates from the total production rates, we estimated the production rates of the unknown Cl_2 sources. Recent studies proposed that nitrate photolysis and aerosol iron photochemistry may serve as significant daytime Cl_2 sources[18,37,47]. Accordingly, we analyzed the correlations between the unknown Cl_2 sources and the approximate values of the nitrate photolysis and aerosol iron photochemistry indicator (Fig. 2c, d), revealing good correlations (r = 0.41 and 0.45), respectively. This suggests that these processes may contribute to additional daytime Cl_2 sources. Notably, although the uptake coefficients for HOCl, $ClNO_2$, OH·, and O_3 are supported by literature[23], they may not be fully applicable to the specific ambient conditions of our study site. Therefore, we have established a series of different scenarios to evaluate variations in unknown sources of Cl_2 (Table S2). As shown in Fig. S8, daytime Cl_2 concentrations could only be reasonably simulated when the uptake coefficients for O_3, $ClNO_2$, HOCl, and OH· were set to four times the literature-reported values. However, we consider these adjusted uptake coefficients to be unrealistically high. Based on scenario analysis, the estimated production rates of the unidentified Cl_2 sources reach up to 0.22 $ppb \cdot h^{-1}$.

HOCl was primarily generated via the reaction of ClO with HO_2·, where ClO is formed from the reaction of Cl· with O_3, though ClO can also be consumed by NO_x. Observational results support this mechanism (Fig. S9), showing a strong correlation between daytime O_3 and HOCl concentrations, with high HOCl levels often coinciding with low NO_x concentrations. The photolysis of $ClNO_2$ and Cl_2 provides a substantial source of Cl·, accelerating HOCl formation via the reaction of ClO and HO_2·. Using the box model, we evaluated the contributions of the ClO + HO_2· reaction and other gas-phase pathways (e.g., $Cl_2/ClNO_2$ + OH·, OH· + OClO) to HOCl concentrations. The results indicate that the simulated HOCl concentrations accounted for only 5–10% of the observed daytime concentrations (Fig. 3a). Similarly, unknown sources of HOCl were also found in marine air affected by ship exhaust in Hong Kong[40] and in the marine boundary layer of the eastern tropical Atlantic[33]. These findings highlight a considerable gap in the current understanding of HOCl sources. In this study, the loss rates of HOCl reached 0.12 $ppb \cdot h^{-1}$, with photolysis as the primary loss pathway (81.0%), followed by HOCl uptake (17.0%) and the reaction of HOCl with OH· (2.0%) (Fig. 3b). Similar to the analysis of unknown Cl_2 sources, we estimated the formation rates of the unknown HOCl sources by subtracting the loss rates from the formation rates. Recent studies suggested that nitrate photolysis and aerosol iron photochemistry not only contribute to Cl_2 formation but may also increase HOCl concentrations[36,37,47,48]. To validate these mechanisms at our study site, we analyzed the correlations between the unknown HOCl sources and the approximate values of the nitrates photolysis and aerosol iron photochemistry indicator (Fig. 3c, d), finding their strong correlations (r = 0.69 and 0.56), respectively. Therefore, in addition to Cl_2, nitrate photolysis and aerosol iron photochemistry also resulted in HOCl formation.

As mentioned before, observed daytime concentrations of $ClNO_2$ could been not explained by heterogeneous N_2O_5 processes when considering large loss rates of $ClNO_2$ during the daytime primarily contributing

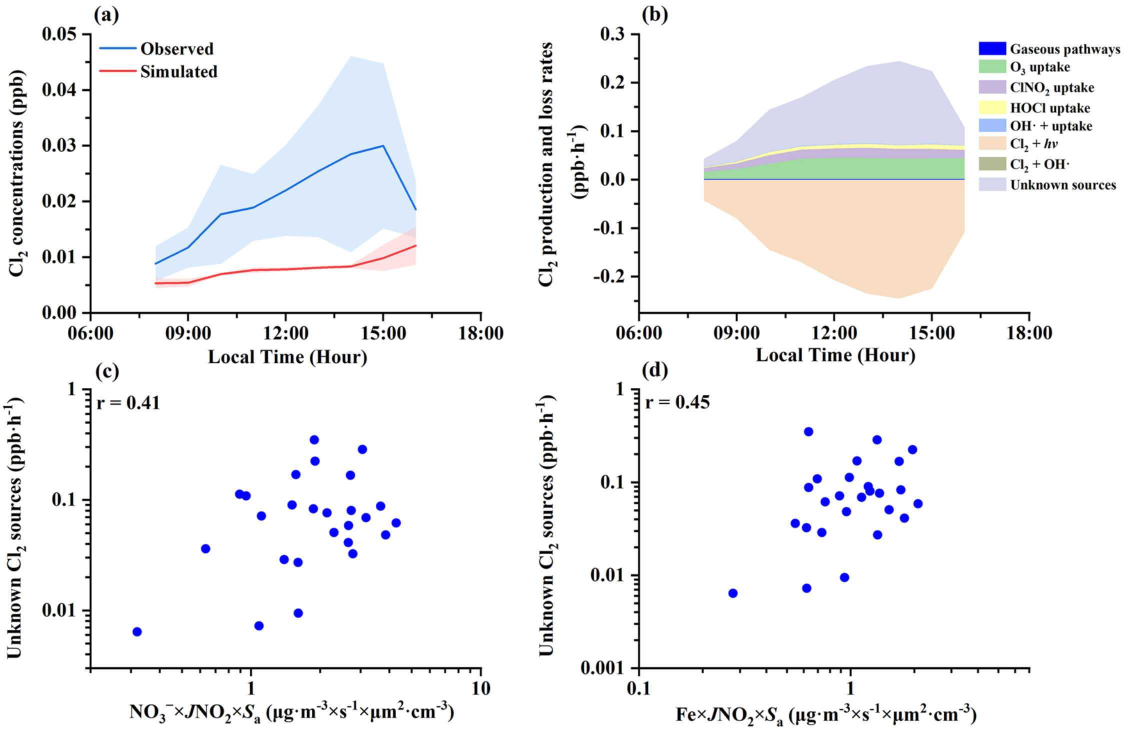

Fig. 2 | Formation mechanisms of Cl_2. **a** Comparison between observed and simulated Cl_2 concentrations; **b** Production and loss rates of Cl_2; **c** Relationship between the unknown sources of Cl_2 and the indicator of nitrate photolysis (NO_3^-×*J*NO_2×S_a); **d** Relationship between the unknown sources of Cl_2 and the indicator of aerosol iron photochemistry (Fe×*J*NO_2×S_a). Here, S_a signifies aerosol surface area.

Fig. 3 | Formation mechanisms of HOCl and $ClNO_2$. **a** Comparison between observed and simulated HOCl concentrations; **b** Production and loss rates of HOCl; **c** Relationship between the unknown sources of HOCl and the indicator of nitrate photolysis (NO_3^-×*J*NO_2×S_a); **d** Relationship between the unknown sources of HOCl and the indicator of aerosol iron photochemistry (Fe×*J*NO_2×S_a); **e** Production and loss rates of $ClNO_2$; **f** Relationship between the unknown sources of $ClNO_2$ and the indicator of nitrate photolysis (NO_3^-×*J*NO_2×S_a).

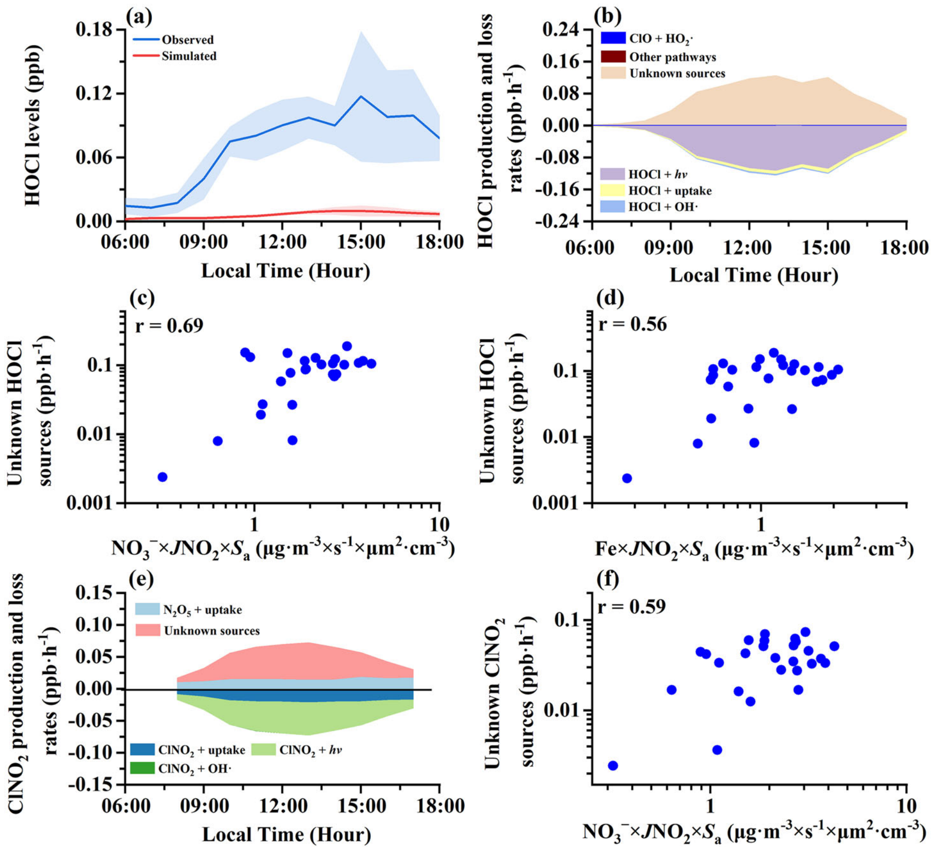

Fig. 4 | Impacts of reactive chlorine chemistry on atmospheric oxidation capacity under the influence of marine and continental air masses, respectively. a Contributions of $ClNO_2$, Cl_2, and HOCl photolysis to Cl· production rates in continental air masses; **b–f** Differences in the contributions of reactive chlorine chemistry to OH· (**b**) HO_2· (**c**) RO_2· (**d**) PA· concentrations (**e**) and net O_3 production rates (net P(O_3)) (**f**) under the influence of marine (Type 1) and continental (Type 2) air masses.

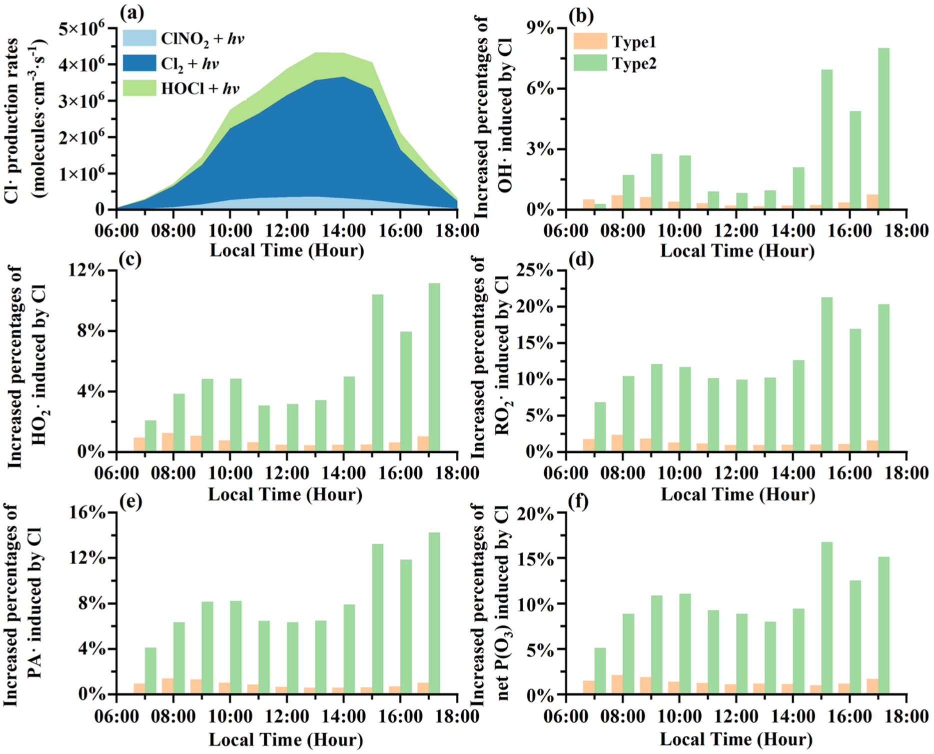

from $ClNO_2$ photolysis and uptake (Fig. 3e), revealing unknown production pathways of daytime $ClNO_2$. Notably, strong correlations among HOCl and $ClNO_2$, Cl_2 during the daytime imply that these species may share similar daytime sources. Recent experimental and modeling studies indicated that nitrate photolysis can produce $ClNO_2$ in addition to Cl_2 and HOCl[48]. Specifically, O(^{3}P) generated by nitrate photolysis oxidizes Cl^- to form Cl_2 and HOCl, further reacting with nitrite to produce $ClNO_2$[48]. In our study, the production rates of unknown $ClNO_2$ sources exhibited a strong correlation with the approximate value of the nitrate photolysis indicator ($r = 0.59$) (Fig. 3f), indicating that nitrate photolysis may be an important source for the elevated daytime $ClNO_2$ concentrations at our study site.

Figure S10 illustrates the daytime chemical cycling mechanisms of $ClNO_2$, Cl_2, and HOCl at our study site. The photolysis of $ClNO_2$, Cl_2, and HOCl releases Cl·, which react with O_3 to form ClO. This ClO subsequently interacts with HO_2·, NO, and NO_2 to produce HOCl, Cl·, and $ClONO_2$, respectively. The heterogeneous uptake of HOCl, $ClNO_2$, O_3, and OH· on chloride-containing aerosol surfaces contributes to the formation of Cl_2. Furthermore, the heterogeneous uptake of N_2O_5 results in the production of $ClNO_2$. Additionally, the photolysis of nitrate facilitates the simultaneous generation of $ClNO_2$, Cl_2, and HOCl, while aerosol iron photochemistry promotes the formation of Cl_2 and HOCl. Overall, these processes significantly enhance reactive chlorine chemistry during the Type 2 period, potentially having profound implications for photochemical oxidation processes.

Enhanced oxidation capacity

Based on the box model, we systematically compared the changes in atmospheric oxidation induced by reactive chlorine chemistry (the photolysis of $ClNO_2$, Cl_2, and HOCl) and their differential impacts on O_3 and PAN formation during the Type 1 and Type 2 periods. The average maximum Cl· production rates increased significantly from 2.7×10^5 molecules·cm^{-3}·s^{-1} during the Type 1 period to 4.5×10^6 molecules·cm^{-3}·s^{-1} during the Type 2 period, representing an approximately 15-fold increase (Fig. S11). As illustrated in Fig. 4a, source analysis revealed that Cl_2 photolysis dominated Cl· production during both periods, contributing over 80%, followed by HOCl photolysis (~15%), with $ClNO_2$ photolysis contributing the least (~5%). Higher contribution from Cl_2 photolysis have also been found in northern and southern China[18,24]. Differently, several previous studies reported larger contribution of $ClNO_2$ photolysis to Cl· generation in the early morning[5,10,49]. However, in this study, the limited nighttime accumulation of $ClNO_2$ resulted in minimal contributions to $ClNO_2$ concentrations in the morning. The contribution of HCl + OH to Cl· generation was not considered in this study based on two key considerations: (1) the absence of direct HCl measurements, and (2) the substantial uncertainties of simulated HCl concentrations.

The Cl· released from the photolysis of $ClNO_2$, Cl_2, and HOCl promoted the formation of HO_2· and RO_2· through VOC oxidation. Consistent with previous studies[18,38], it is found that Cl· primarily participated in alkane oxidation (>50%), followed by the oxidation of OVOCs and alkenes (Fig. S12). Notably, HOCl photolysis not only releases Cl· but also generates OH·. Additionally, HO_2· and RO_2· generated by chlorine chemistry can react with NO to form OH·, which further promotes HO_2· and RO_2· formation through VOC oxidation, thereby intensifying the cycling of OH·, HO_2· and RO_2·. During the Type 1 period, low concentrations of $ClNO_2$, Cl_2, and HOCl resulted in limited enhancement of OH· (1.4%), HO_2· (<1.0%), and RO_2· (<1.0%) concentrations via Cl·-mediated VOC oxidation (Fig. 4b–d). In contrast, during the Type 2 period, higher concentrations of reactive chlorine compounds led to average increases of 3.0%, 5.4%, and 13.0% in OH·, HO_2· and RO_2· concentrations, respectively. Importantly, the concentrations of PA· within RO_2· increased markedly during the Type 2 period due to enhanced reactive chlorine chemistry, with an average maximum increase of 14.2% (Fig. 4e).

Based on these changes in radical concentrations, we further quantified the impacts of reactive chlorine chemistry on photochemical O_3 and PAN formation. By calculating the difference between O_3 production and loss rates, we assessed its effect on net O_3 production rates (P(O_3)): the average increase was 1.4% during the Type 1 period but rose to 10.5% during the Type 2 period (Fig. S13 and Fig. 4f). Simultaneously, as PAN is formed through the reaction of PA· with NO_2, the increased PA· concentrations induced by reactive chlorine chemistry greatly enhanced PAN concentrations, with a maximum increase of 14.1% during the Type 2 period.

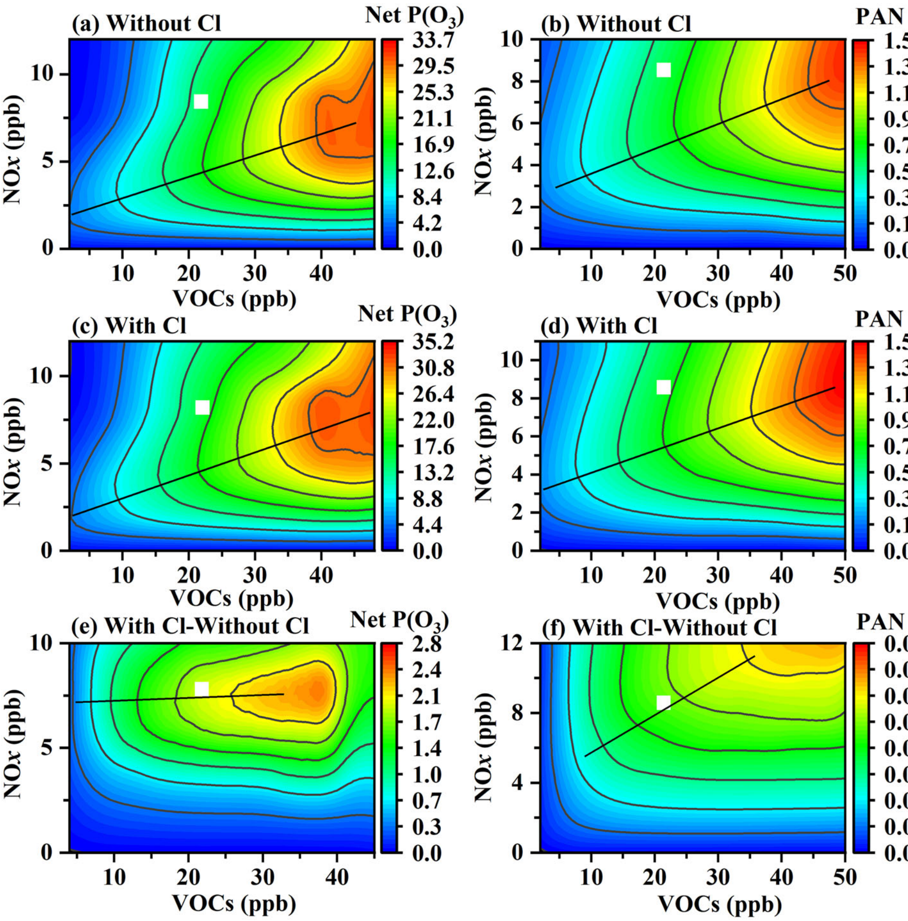

Fig. 5 | EKMA curves of net O_3 production rates (net P(O_3), ppb·h^{-1}) and PAN concentrations (ppb) under different simulation scenarios during the Type 2 period. (**a**, **c**, **e**) Net P(O_3) (Unit: ppb·h^{-1}); (**b**, **d**, **f**) PAN concentrations (Unit: ppb). (**a**, **b**) Scenarios without reactive chlorine species constraints; (**c,d**) scenarios constrained by $ClNO_2$, Cl_2, and HOCl; (**e,f**) the individual impacts of chlorine chemistry on O_3 and PAN (△Cl). △Net P(O_3) equals net P(O_3) with chlorine chemistry minus net P(O_3) without chlorine chemistry, and △PAN equals PAN concentrations with chlorine chemistry minus PAN concentrations without chlorine chemistry. The white squares in the Fig. 5 represent the average concentrations of VOCs and NO*x* during the Type 2 period.

The sensitivity of O_3 and PAN generation

Several studies have revealed the role of reactive chlorine chemistry in modulating O_3 production sensitivity[5,50,51], yet its contribution to PAN formation sensitivity remains unclear. Therefore, we evaluated the impacts of VOC and NO*x* reduction on net P(O_3) and PAN concentrations after incorporating reactive chlorine chemistry mechanisms into the box model (Fig. 5).

Given higher O_3 and PAN concentrations during the Type 2 period and the significant enhancement effect of reactive chlorine chemistry during this period, we focused on assessing its impacts on EKMA curves for net P(O_3) and PAN concentrations during the Type 2 period. The results show that in scenarios without reactive chlorine chemistry, O_3 and PAN generation is primarily controlled by VOCs, and a reduction in NO*x* concentrations exacerbates their formation (Fig. 5a, b). Further analysis reveals that when reactive chlorine chemistry is introduced into the box model (Fig. 5c, d), although O_3 and PAN production remains predominantly VOC-sensitive, net P(O_3) and PAN concentrations increased, highlighting the strong influence of reactive chlorine chemistry on photochemical oxidation processes. To directly compare the effects of including or excluding reactive chlorine chemistry on O_3 and PAN production, we conducted a difference analysis of net P(O_3) and PAN concentrations between scenarios with and without reactive chlorine species constraints and subsequently generated EKMA curves based on this analysis. Notably, when reactive chlorine chemistry is considered, the sensitivity of O_3 and PAN shifts to co-control by VOCs and NO*x* (Fig. 5e, f). This result underscores the critical role of VOCs and NO*x* in the positive impact of reactive chlorine chemistry on photochemical O_3 and PAN production.

Previous studies based on seasonal observations of $ClNO_2$ and Cl_2 in Beijing have shown that the inclusion of reactive chlorine chemistry alters O_3 sensitivity[5]. Research in southern coastal China also indicated that Cl_2 generated from nitrates photolysis limits O_3 increases in VOC-sensitive regions and exacerbates O_3 decreases in NO*x*-sensitive regions[51]. However, these studies did not comprehensively consider reactive chlorine species, thereby, potentially resulting in the underestimation for the effects of reactive chlorine chemistry in atmospheric oxidation. Notably, previous studies indicated that the molybdenum conversion method tends to overestimate NO_2 concentrations[52–54], which may affect the sensitivity of O_3 and PAN formation. To evaluate this uncertainty, we reduced the observed concentrations of NO_2 by 20%. As shown in Fig. S14, compared with the original results, the decreased concentrations of NO_2 indeed altered the sensitivity of O_3 and PAN formation.

In summary, this study revealed that the elevated concentrations of precursors promoted the formation of reactive chlorine species by accelerating heterogeneous chemical processes. The pollution-driven chlorine chemistry moderately enhanced atmospheric oxidation capacity, resulting in O_3 and PAN formation and shifting their control regime. Importantly, we identified unknown sources of reactive chlorine species linked to nitrate photolysis and aerosol iron photochemistry. However, the lack of well-constrained parameterization schemes for these heterogeneous processes limits the accurate quantification of their contributions. Future research should prioritize elucidating these mechanisms to refine parameterizations and improve the precision of model simulations, thereby advancing our understanding of reactive chlorine chemistry in the atmospheric environment.

In our previous studies on Cl_2 and HOCl during the autumn[36,39], the impacts of different air mass sources on the distributions of reactive chlorine species were not well revealed due to the constant influence of coastal air masses during this period. However, in this study, by systematically comparing the distribution patterns and photochemical impacts of reactive chlorine species under the influence of marine and continental air masses, this study emphasized the pivotal role of anthropogenic pollutants in driving reactive chlorine chemistry, with important implications for air pollution control policies. Although sea salt aerosols serve as an abundant source of particulate chloride, they are not the primary limiting factor for the generation of reactive chlorine species[18,36]. Instead, anthropogenic emissions, particularly NO*x* and iron-containing aerosols, play a critical role in the chlorine chemistry. These findings underscore the necessity of strict controls on anthropogenic pollutants (e.g., VOCs, NO*x*, and Fe) to mitigate chlorine-mediated adverse environmental impacts. Furthermore, we propose extending control measures to anthropogenic chlorine emissions in air pollution mitigation strategies in the future.

Methods

Field Measurements

Measurements of reactive chlorinated compounds and associated parameters were conducted from July 19th to August 9th, 2023, in Xiamen, a major coastal city in Southeast China. The study site, located over 70 meters above ground level in an urban area, is surrounded by Xinglin Bay, educational and residential buildings, and traffic roads. Throughout the observation period, $ClNO_2$, Cl_2, HOCl, N_2O_5, VOCs, and other trace gases (including NO*x*, CO, SO_2, and O_3), as well as $PM_{2.5}$, aerosol chemical components (e.g., Fe and water-soluble ions), aerosol surface area (S_a), and meteorological parameters, were monitored at the site. Detailed descriptions of observation instruments are provided in Text S2.

An iodide-adduct Chemical Ionization-Atmospheric Pressure Interface-Time of Flight mass spectrometer (I^--ToF-CIMS) was employed to measure $ClNO_2$, Cl_2, HOCl, and N_2O_5. The operational principles of I^--ToF-CIMS and related details have been described in previous studies and Text S1[36,38,55]. Targeted species selectively reacted with reagent ions (I^- and $I(H_2O)^-$), forming iodide clusters that were detected by the mass spectrometer. Calibrations of $ClNO_2$, Cl_2, HOCl, and N_2O_5 were performed using established methods[7,18,19,22,33,56]. Briefly, $ClNO_2$ was synthesized through the reaction of Cl_2 with a moistened mixture of $NaNO_2$ and NaCl. N_2O_5 was generated by the reaction of O_3 with an excess of NO_2. Cl_2 was produced using a Cl_2 permeation tube (supplied by VICI Metronics, Inc.) with a permeation rate of 98 $ng{\cdot}min^{-1}$. HOCl calibration was achieved by converting HOCl to Cl_2. By analyzing the reduction in the HOCl signal and the corresponding increase in the Cl_2 signal as they passed through a chloride solution, the relative sensitivities of HOCl and Cl_2 were determined. A summary of the calibration procedures and uncertainty analysis is provided in Text S3 and Fig. S15.

The box model

An observation-based model (OBM) was employed to investigate the effects of $ClNO_2$, Cl_2, and HOCl photolysis on photochemical oxidation processes. The box model incorporated the Master Chemical Mechanism (MCM Version 3.3.1) and integrated established chlorine chemistry mechanisms based on previous studies[18,49]. Detailed configurations of the box model have been thoroughly described in our earlier publications[38,57]. The photolysis rates of $ClNO_2$, Cl_2, and HOCl ($JClNO_2$, JCl_2, and $JHOCl$) were derived from the Tropospheric Ultraviolet and Visible Radiation (TUV) model under clear-sky conditions, with adjustments made using measured JNO_2 values at our study site. In this study, the box model was constrained by observed data, including $ClNO_2$, Cl_2, HOCl, VOCs, HCHO, HONO, O_3, NO_2, NO, CO, SO_2, and meteorological parameters, all provided at 1 h time resolution, ensuring consistency between the simulated and observed diurnal variations of these species' concentrations.

Notably, the dissociation of N_2O_5 into NO_2^+ and NO_3^- initiates competitive reactions between Cl^- and other species with NO_2^+, which directly modulates $ClNO_2$ production[41]. Following previous studies[6,58], we employed the simplified reaction ($N_2O_5 + Cl^- \rightarrow ClNO_2$) in our model, while addressing potential uncertainties through varying N_2O_5 uptake coefficients and $ClNO_2$ yields. Quantifying Cl_2 and HOCl sources and accurately simulating their observed concentrations remain a great challenge in reactive chlorine chemistry. Existing studies have yet to fully resolve their sources or achieve precise simulations of these species' concentrations[40,58]. Our study accordingly distinguishes between the known and unknown sources. For the known sources, we quantified formation and loss rates using established laboratory parameterizations. Sensitivity analysis was performed by testing different uptake coefficients and yields. The unknown source strength was derived by subtracting known formation rates from total production, followed by correlation analysis with potential mechanisms to assess their possibility.

Based on the box model, this study analyzed the generation of OH·, HO_2·, RO_2·, O_3, and PAN under the influence of marine and continental air masses. To quantify the effects of chlorine chemistry on atmospheric oxidation processes, two distinct chemical scenarios were examined: one incorporating the reactive chlorine chemistry mechanism and another excluding it. To further elucidate the impacts of reactive chlorine chemistry on the control strategies for O_3 and PAN precursors, we employed the empirical kinetic modeling approach (EKMA) during the period dominated by continental air masses, which are typically associated with enhanced photochemical pollution. Through a comprehensive 20 × 20 concentration matrix, this study quantitatively simulated the response patterns of O_3 and PAN formation across a wide range of concentration gradients (both reduction and increase) for VOCs and NO*x*. Additionally, we conducted a mechanistic analysis to evaluate the relative contributions of current atmospheric processes, including (1) gaseous reactions and heterogeneous uptake of $ClNO_2$, HOCl, OH·, and O_3, (2) $ClO + HO_2$· and other gaseous reactions, and (3) heterogeneous N_2O_5 uptake, to the daytime concentrations of Cl_2, HOCl, and $ClNO_2$, respectively. Detailed descriptions of the model configurations, input parameters, heterogeneous reaction settings, and output parameters are provided in Text S1.

HYSPLIT backward trajectory

The 24 h backward trajectories of air masses arriving at 500 meters above ground level were calculated using the Hybrid Single-Particle Lagrangian Integratesd Trajectory (HYSPLIT) model.

Data availability

The data in our study are available from the corresponding author on reasonable request.

Code availability

The codes in our study are available from the corresponding author on reasonable request.

Received: 8 May 2025; Accepted: 13 June 2025;

References

1. Li, Q. et al. Potential effect of halogens on atmospheric oxidation and air quality in China. *J. Geophys. Res. Atmos.* **125**, e2019JD032058 (2020).
2. Li, Q. et al. Reactive halogens increase the global methane lifetime and radiative forcing in the 21st century. *Nat. Commun.* **13**, 2768 (2022).
3. Li, Q. et al. Halogens enhance haze pollution in China. *Environ. Sci. Technol.* **55**, 13625–13637 (2021).
4. Yi, X., et al. Significant impact of reactive chlorine on complex air pollution over the yangtze river delta region, China. *J. Geophys. Res. Atmos.* **128**, e2023JD038898 (2023).
5. Ma, W. et al. Reactive chlorine species advancing the atmospheric oxidation capacities of inland urban environments. *Environ. Sci. Technol.* **57**, 14638–14647 (2023).
6. Tham, Y. J. et al. Significant concentrations of nitryl chloride sustained in the morning: investigations of the causes and impacts on ozone production in a polluted region of northern China. *Atmos. Chem. Phys.* **16**, 14959–14977 (2016).
7. Wang, H. et al. Formation and impacts of nitryl chloride in Pearl River Delta. *Atmos. Chem. Phys.* **22**, 14837–14858 (2022).

8. Thornton, J. A. et al. A large atomic chlorine source inferred from mid-continental reactive nitrogen chemistry. *Nature* **464**, 271–274 (2010).
9. Osthoff, H. D. et al. High levels of nitryl chloride in the polluted subtropical marine boundary layer. *Nat. Geosci.* **1**, 324–328 (2008).
10. Phillips, G. J. et al. Significant concentrations of nitryl chloride observed in rural continental Europe associated with the influence of sea salt chloride and anthropogenic emissions. *Geophys. Res. Lett.* **39**, L10811 (2012).
11. Riedel, T. P. et al. Nitryl chloride and molecular chlorine in the coastal marine boundary layer. *Environ. Sci. Technol.* **46**, 10463–10470 (2012).
12. Riedel, T. P. et al. Chlorine activation within urban or power plant plumes: Vertically resolved $ClNO_2$ and Cl_2 measurements from a tall tower in a polluted continental setting. *J. Geophys. Res. Atmos.* **118**, 8702–8715 (2013).
13. Bannan, T. J. et al. The first UK measurements of nitryl chloride using a chemical ionization mass spectrometer in central London in the summer of 2012, and an investigation of the role of Cl atom oxidation. *J. Geophys. Res. Atmos.* **120**, 5638–5657 (2015).
14. Bannan, T. J. et al. Ground and airborne U.K. measurements of nitryl chloride: an investigation of the role of cl atom oxidation at weybourne atmospheric observatory. *J. Geophys. Res. Atmos.* **122**, 11,154–111,165 (2017).
15. Jeong, D. et al. Integration of airborne and ground observations of nitryl chloride in the Seoul metropolitan area and the implications on regional oxidation capacity during KORUS-AQ 2016. *Atmos. Chem. Phys.* **19**, 12779–12795 (2019).
16. Li, F. et al. Observation of nitrogen oxide-influenced chlorine chemistry and source analysis of Cl_2 in the Yangtze River Delta, China. *Atmos. Environ.* **306**, 119829 (2023).
17. Mielke, L. H. et al. Heterogeneous formation of nitryl chloride and its role as a nocturnal NO_x reservoir species during CalNex-LA 2010. *J. Geophys. Res. Atmos.* **118**, 10,638–610,652 (2013).
18. Peng, X. et al. Photodissociation of particulate nitrate as a source of daytime tropospheric Cl_2. *Nat. Commun.* **13**, 1–10 (2022).
19. Wang, T. et al. Observations of nitryl chloride and modeling its source and effect on ozone in the planetary boundary layer of southern China. *J. Geophys. Res. Atmos.* **121**, 2476–2489 (2016).
20. Niu, Y.-B., et al. Fast nocturnal heterogeneous chemistry in a coastal background atmosphere and its implications for daytime photochemistry. *J. Geophys. Res. Atmos.* **127**, e2022JD036716 (2022).
21. Xia, M. et al. Winter $ClNO_2$ formation in the region of fresh anthropogenic emissions: seasonal variability and insights into daytime peaks in northern China. *Atmos. Chem. Phys.* **21**, 15985–16000 (2021).
22. Mattila, J. M. et al. Multiphase chemistry controls inorganic chlorinated and nitrogenated compounds in indoor air during bleach cleaning. *Environ. Sci. Technol.* **54**, 1730–1739 (2020).
23. Xia, M. et al. Significant production of $ClNO_2$ and possible source of Cl_2 from N_2O_5 uptake at a suburban site in eastern China. *Atmos. Chem. Phys.* **20**, 6147–6158 (2020).
24. Liu, X. et al. High levels of daytime molecular chlorine and nitryl chloride at a rural site on the North China plain. *Environ. Sci. Technol.* **51**, 9588–9595 (2017).
25. Liao, J. et al. High levels of molecular chlorine in the Arctic atmosphere. *Nat. Geosci.* **7**, 91–94 (2014).
26. Knipping, E. et al. Experiments and simulations of ion-enhanced interfacial chemistry on aqueous NaCl aerosols. *Science* **288**, 301–306 (2000).
27. Oum, K. W., Lakin, M., DeHaan, D. O., Brauers, T. & Finlayson-Pitts, B. J. J. S. Formation of molecular chlorine from the photolysis of ozone and aqueous sea-salt particles. *Science* **279**, 74–76 (1998).
28. Faxon, C., Bean, J. & Ruiz, L. Inland concentrations of Cl_2 and $ClNO_2$ in Southeast Texas suggest chlorine chemistry significantly contributes to atmospheric reactivity. *Atmosphere* **6**, 1487–1506 (2015).
29. Lim, M., Chiang, K. & Amal, R. Photochemical synthesis of chlorine gas from iron(III) and chloride solution. *J. Photochem. Photobiol. A Chem.* **183**, 126–132 (2006).
30. Li, Y. et al. Photoinduced production of chlorine molecules from titanium dioxide surfaces containing chloride. *Environ. Sci. Technol. Lett.* **7**, 70–75 (2020).
31. Roberts, J. M., Osthoff, H. D., Brown, S. S. & Ravishankara, A. R. N_2O_5 oxidizes chloride to Cl_2 in acidic atmospheric aerosol. *Science* **321**, 1059 (2008).
32. Haskins, J. D. et al. Observational constraints on the formation of Cl_2 from the reactive uptake of $ClNO_2$ on aerosols in the polluted marine boundary layer. *J. Geophys. Res. Atmos.* **124**, 8851–8869 (2019).
33. Lawler, M. J. et al. HOCl and Cl_2 observations in marine air. *Atmos. Chem. Phys.* **11**, 7617–7628 (2011).
34. McNamara, S. M. et al. Springtime nitrogen oxide-influenced chlorine chemistry in the coastal arctic. *Environ. Sci. Technol.* **53**, 8057–8067 (2019).
35. Yan, C. et al. Increasing contribution of nighttime nitrogen chemistry to wintertime haze formation in Beijing observed during COVID-19 lockdowns. *Nat. Geosci.* **16**, 975–981 (2023).
36. Chen, G. et al. HOCl formation driven by photochemical processes enhanced atmospheric oxidation capacity in a coastal atmosphere. *Environ. Sci. Technol.* **59**, 5164–5171 (2025).
37. van Herpen, M. M. J. W. et al. Photocatalytic chlorine atom production on mineral dust–sea spray aerosols over the North Atlantic. *Proc. Natl. Acad. Sci. USA* **120**, e2303974120 (2023).
38. Chen, G. et al. Increasing contribution of chlorine chemistry to wintertime ozone formation promoted by enhanced nitrogen chemistry. *Environ. Sci. Technol.* **58**, 22714–22721 (2024).
39. Chen, G. et al. Driving factors and photochemical impacts of Cl_2 in coastal atmosphere of Southeast China. *npj Clim. Atmos. Sci.* **8**, 135 (2025).
40. Xia, M. et al. Chlorine activation in marine air: insights from chemical budgets of molecular chlorine and hypochlorous acid. *J. Geophys. Res. Atmos.* **130**, e2024JD042568 (2025).
41. Soni, M. et al. Comprehensive multiphase chlorine chemistry in the box model CAABA/MECCA: implications for atmospheric oxidative capacity. *Atmos. Chem. Phys.* **23**, 15165–15180 (2023).
42. Brown, S. S. et al. Aircraft observations of daytime NO_3 and N_2O_5 and their implications for tropospheric chemistry. *J. Photochem. Photobiol. A Chem.* **176**, 270–278 (2005).
43. Geyer, A. et al. Direct observations of daytime NO_3: implications for urban boundary layer chemistry. *J. Geophys. Res. Atmos*. **108**, 2967 (2003).
44. McDuffie, E. E. et al. $ClNO_2$ yields from aircraft measurements during the 2015 WINTER campaign and critical evaluation of the current parameterization. *J. Geophys. Res. Atmos.* **123**, 12,994–913,015 (2018).
45. McDuffie, E. E. et al. Heterogeneous N_2O_5 uptake during winter: aircraft measurements during the 2015 WINTER campaign and critical evaluation of current parameterizations. *J. Geophys. Res. Atmos.* **123**, 4345–4372 (2018).
46. Qiu, X. et al. Significant impact of heterogeneous reactions of reactive chlorine species on summertime atmospheric ozone and free-radical formation in North China. *Sci. Total Environ.* **693**, 133580 (2019).
47. Chen, Q. et al. Impact of molecular chlorine production from aerosol iron photochemistry on atmospheric oxidative capacity in North China. *Environ. Sci. Technol.* **58**, 12585–12597 (2024).
48. Dalton, E. Z. et al. Daytime atmospheric halogen cycling through aqueous-phase oxygen atom chemistry. *J. Am. Chem. Soc.* **145**, 15652–15657 (2023).

49. Xue, L. K. et al. Development of a chlorine chemistry module for the master chemical mechanism. *Geosci. Model Dev.* **8**, 3151–3162 (2015).
50. Li, Q. et al. “New” reactive nitrogen chemistry reshapes the relationship of ozone to its precursors. *Environ. Sci. Technol.* **52**, 2810–2818 (2018).
51. Dai, J. et al. Significant impact of a daytime halogen oxidant on coastal air quality. *Environ. Sci. Technol.* **59**, 2169–2180 (2025).
52. Fehsenfeld, F. C. et al. A ground-based intercomparison of NO, NO*x*, and NO*y* measurement techniques. *J. Geophys. Res. Atmos.* **92**, 14710–14722 (1987).
53. Xu, Z. et al. Evaluating the uncertainties of thermal catalytic conversion in measuring atmospheric nitrogen dioxide at four differently polluted sites in China. *Atmos. Environ.* **76**, 221–226 (2013).
54. Zhang, Y. et al. Biogenic volatile organic compounds enhance ozone production and complicate control efforts: Insights from long-term observations in Hong Kong. *Atmos. Environ.* **309**, 119917 (2023).
55. Ye, C. et al. Chemical characterization of oxygenated organic compounds in the gas phase and particle phase using iodide CIMS with FIGAERO in urban air. *Atmos. Chem. Phys.* **21**, 8455–8478 (2021).
56. Thaler, R. D., Mielke, L. H. & Osthoff, H. D. Quantification of Nitryl Chloride at part per trillion mixing ratios by thermal dissociation cavity ring-down spectroscopy. *Anal. Chem.* **83**, 2761–2766 (2011).
57. Chen, G. et al. Photochemical pollution during summertime in a coastal city of Southeast China: ozone formation and influencing factors. *Atmos. Res.* **301**, 107270 (2024).
58. Chen, Q. et al. Large daytime molecular chlorine missing source at a suburban site in East China. *J. Geophys. Res. Atmos.* **127**, e2021JD035796 (2022).

Acknowledgements

This study was funded by the National Natural Science Foundation of China (U22A20578), the guiding project of seizing the commanding heights of “self-purifying city” (NO. IUE-CERAE-202402), the National Key Research and Development Program (2022YFC3700304), the Science and Technology Department of Fujian Province (2022L3025), STS Plan Supporting Project of the Chinese Academy of Sciences in Fujian Province (2023T3013), and Xiamen Atmospheric Environment Observation and Research Station of Fujian Province.

Author contributions

G.C. and J.C. co-designed this study. G.C. analyzed the data and wrote the manuscript, with J.C. providing funding and revisions. L.X. and X.F. assisted in field observations, and all authors (G.C., J.C., L.X., Z.C., Y.Z., X.F., Z.L., and X.J.) participated in research discussions.

Competing interests

The authors declare no competing interests.

Additional information

Supplementary information The online version contains supplementary material available at https://doi.org/10.1038/s41612-025-01133-6.

Correspondence and requests for materials should be addressed to Lingling Xu or Jinsheng Chen.

Reprints and permissions information is available at http://www.nature.com/reprints